Article

J. Biol. Regul. Homeost. Agents. 2024; 38(5): 4209–4221
https://doi.org/10.23812/j.biol.regul.homeost.agents.20243805.334

BARD1 Deletion Suppresses Progression of Colorectal Cancer through Regulation of *SLIT3*/Cyclin D3

Yongwei Zhuang[1,†], Shufang Ye[1,*,†], Yangyang Liu[1], Bin Chen[2], Yanjiao Wang[2], Zengli Zhou[2]

[1]Digestive Endoscopy Center, Lishui City People's Hospital, 323020 Lishui, Zhejiang, China
[2]Digestive Internal Medicine Department, Lishui City People's Hospital, 323020 Lishui, Zhejiang, China
*Correspondence: yeshufang_ysf@163.com (Shufang Ye)
[†]These authors contributed equally.
Published: 1 May 2024

Background: Breast-cancer susceptibility gene 1 (BRCA1) associated RING domain 1 (*BARD1*) expression is upregulated in colorectal cancer (CRC), and its mutation forms are also related to clinical prognosis of the cancer. The primary focus of this study is to delineate the mechanism of *BARD1* underlying the development and progression of CRC.
Methods: *BARD1* expression pattern in CRC was uncovered by quantitative real-time reverse transcription polymerase chain reaction (qRT-PCR) with the aid of bioinformatics means. Following transfection of small interfering RNA targeting *BARD1* (si*BARD1*) and short hairpin RNA against slit guidance ligand 3 (*SLIT3*; sh*SLIT3*), CRC cell viability, proliferation, apoptosis, migration, and invasion were measured by cell counting kit-8 assay, colony formation assay, flow cytometry, wound healing assay, and Transwell assay. To verify how *BARD1* impacts *SLIT3* degradation, CRC cells were treated with cycloheximide (CHX) for different periods of time (0, 2, 4, 6, 8 h). After administration of si*BARD1*-transfected CRC cells or blank treatment into Balb/c nude mice, the tumor volume and weight of the animals were determined, followed by quantification of cyclin D3 (immunohistochemistry) and corresponding genes/proteins (qRT-PCR and western blotting).
Results: *BARD1* expression was upregulated in CRC cells ($p < 0.001$). Si*BARD1* reduced cell viability, proliferation, migration and invasion; increased apoptosis; upregulated E-cadherin level; and downregulated N-cadherin, Snail, and cyclin D3 levels in CRC cells ($p < 0.05$). In contrast, sh*SLIT3* presented an opposite effect on these indexes in CRC cells ($p < 0.05$). Si*BARD1* suppressed the degradation of *SLIT3*, hampered tumor growth, reduced cyclin D3 expression, and promoted *SLIT3* expression *in vivo* ($p < 0.001$). Additionally, sh*SLIT3* was found to reverse the effects of si*BARD1*, and vice versa ($p < 0.05$).
Conclusion: *BARD1* deletion stifled the progression of CRC *in vitro* and *in vivo* by upregulating *SLIT3* expression and inhibiting cyclin D3 expression, corroborating *BARD1* as a potential biomarker in CRC carcinogenesis.

Keywords: *BRCA1 associated RING domain 1*; colorectal cancer; *slit guidance ligand 3*; cyclin D3; epithelial mesenchymal transition

Introduction

As a significant health threat to humans, colorectal cancer (CRC) is currently the third most common malignant tumor of the digestive tract [1]. Central to the life-threatening traits of this cancer are metastasis and recurrence [2,3]. It has been reported that genetic mutations, unhealthy dietary habits, weakened immune defenses, and unfavorable lifestyle jointly contribute to the occurrence of CRC [4]. At present, the mainstay of CRC treatment includes molecular targeted therapy, surgery, immunotherapy, and radiotherapy [5,6]. Despite progressive strides being made, the current therapeutic efforts are grappling with challenges such as drug resistance and tumor recurrence, which demand particular clinical attention.

BRCA1 associated RING domain 1 (*BARD1*), which was discovered in 1996, is considered a promising therapeutic target for breast-cancer susceptibility gene 1 (*BRCA1*) mutation-negative cancers on the basis of its interaction with *BRCA1* [7]. A prior study has elucidated that *BARD1* presents as an oncogene or a tumor inhibitor in the development of cancers [8]. Also, *BRCA1*/*BARD1* heterodimer restricts ubiquitin ligase from influencing cell cycle and hormone signaling, and prevents it from causing DNA damage [9,10]. It has been found that *BRCA1*/*BARD1* achieves tumor inhibition through ubiquitination pathway [11]. A growing body of research has contributed to deciphering the influence of *BARD1* on an assortment of cancers. Abnormal *BARD1* isoforms play a role in tumorigenesis of breast and ovarian cancers, and their expressions are related to the reduced survival rate of cancer patients [12]. More importantly, *BARD1* expression is upregulated in CRC, and its mutation forms are linked to the clinical prognosis [13]. Nevertheless, how *BARD1* impacts malignant behaviors of CRC cells and the underlying mechanisms remain to be explored.

Journal of
BIOLOGICAL REGULATORS
and Homeostatic Agents

BRCA1/BARD1 complex functions as E3 ubiquitin ligase, which can modify the proteins [14]. According to the Ubibrowser database (http://ubibrowser.bio-it.cn/ubibrowser_v3/), slit guidance ligand 3 (*SLIT3*) is one of the *BARD1* substrates. *SLIT3* is downregulated in CRC [15], and can hinder the development of breast cancer [16]. Repression of *SLIT3* induces chemoresistance in hepatocellular carcinoma (HCC) through upregulation of cyclin D3 [17], which has been underlined to accelerate the progression of CRC [18].

Taken together, these prior findings contributed to a hypothesis that *BARD1* promotes CRC progression through regulation of *SLIT3*/cyclin D3. Therefore, the current study aimed to explore the effect of *BARD1* on the progression of CRC and its regulatory relationship with *SLIT3*/cyclin D3 by means of *in vivo* and *in vitro* analyses.

Materials and Methods

Bioinformatics

BARD1 expression pattern in CRC was retrieved from University of Alabama at Birmingham Cancer Data Analysis Portal (UALCAN) database (https://ualcan.path.uab.edu/index.html). The correlation between *BARD1* and cell cycle or DNA replication was analyzed by Gene Set Enrichment Analysis (GSEA, https://www.gsea-msigdb.org/). *BARD1* expression across different cancers was analyzed using Tumor Immune Estimation Resource (TIMER; https://cistrome.shinyapps.io/timer/).

Cell Culture and Transfection

Human CRC cell lines (Lovo [CCL-229], HCT116 [CCL-247EMT], SW480 [CCL-228], HCT15 [CCL-225]), human intestinal epithelial cell line (HIEC-6 [CRL-3266]), and human colon tissue cells (CCD-18Co [CRL-1459]) were all obtained from American Type Culture Collection (Manassas, VA, USA). These cells were incubated in Roswell Park Memorial Institute-1640 medium (12633012, Thermo Fisher Scientific, Waltham, MA, USA) supplemented with 10% fetal bovine serum (FBS; C0235, Beyotime, Shanghai, China) at the environment of 5% CO_2 and 37 °C.

Small interfering RNA targeting *BARD1* (si*BARD1*, forward, 5′-AGAUUUGAAAAGAUUCUGCCG-3′; reverse, 5′-GCAGAAUCUUUUCAAAUCUUC-3′) and its negative control (siNC, forward, 5′-CCTAAGGTTAAGTCGCCCTCG-3′; reverse, 5′-GGATTCCAATTCAGCGGGAGC-3′) were constructed using GenePharma (A10001, Shanghai, China). Also, short hairpin RNA against *SLIT3* (sh*SLIT3*, sense: 5′-GCAGGAAGAGTTCAGTTAA-3′; antisense, 5′-TTAACTGAACTCTTCCTGC-3′) was synthetized by GenePharma (China) using plasmids pGPU60 (C01001), while its negative control (shNC, forward, 5′-CAACAAGATGAAGAGCACCAA-3′; reverse, 5′-GTTGTTCTACTTCTCGTGGTT-3′) was also prepared. Transfection was performed, using Lipofectamine™ 3000 reagent (L3000015, Thermo Fisher Scientific, Waltham, MA, USA), on HCT116 and SW480 cells upon reaching 90% confluence in a 96-well plate. Lipofectamine™ 3000 reagent, siRNA, and shRNA were diluted in Opti-MEM™ medium (31985062, Thermo Fisher Scientific, Waltham, MA, USA), respectively. Next, shRNA was mixed with P3000 reagent, and then siRNA/shRNA was transferred into the tubes containing diluted Lipofectamine™ 3000 reagent, after which the mixtures were incubated for 10 min at room temperature. Finally, upon addition of gene-lipid complexes to each well, the cells were subjected to 48-h incubation at 37 °C. All cell samples were routinely tested for STR identification and mycoplasma contamination and were confirmed to be mycoplasma-free.

Cell Treatment

To verify the effects of *BARD1* on *SLIT3* degradation, HCT116 and SW480 cells were reacted with cycloheximide (CHX, 0.2 mg/mL; HY-12320, MedChemExpress, Monmouth Junction, NJ, USA), an inhibitor of protein synthesis, for different periods of time (0, 2, 4, 6, 8 h) at 37 °C. *SLIT3* expression in these cells was evaluated by western blotting at the indicated time points.

Cell Counting Kit-8 Assay

HCT116 and SW480 cell viability was evaluated utilizing cell counting kit-8 (CCK-8) assay kit (Nanjing Jiancheng Bioengineering Institute, Nanjing, China). Briefly, 100 μL HCT116 and SW480 cell suspensions (5×10^3 cells/well) were cultured in a 96-well plate for 24, 48 and 72 h, followed by another 4 h incubation with 10 μL CCK-8 solution. Finally, absorbance (450 nm) reading was accomplished with Infinite M200 Microplate Reader (Tecan, Männedorf, Switzerland).

Colony Formation Assay

HCT116 and SW480 cells (1×10^3 cells/well) cultivated in 6-well plates for 14 days were fixed with methanol (A506806, Sangon Biotech, Shanghai, China) at room temperature for 15 min and subsequently stained by crystal violet staining solution (G1063, Solarbio, Beijing, China) for 3 min. Finally, the colonies were visualized using DSC-H300 compact camera (SONY, Tokyo, Japan), and the rate was calculated using ColonyArea plugin of ImageJ (v. 5.0, Bio-Rad, Hercules, CA, USA). The data in the experimental groups were normalized to the data in the control group.

Flow Cytometry

HCT116 and SW480 cell apoptosis was measured using flow cytometry coupled with Annexin V-FITC Apoptosis Detection Kit (CA1020, Solarbio, Beijing, China). In detail, 100 μL cell suspension (2×10^2 cells/mL) acquired by centrifugation and suspension in binding buffer

was mixed with 5 µL Annexin V-fluorescein isothiocyanate (V-FITC), after which the mixture was incubated for 5 min in the dark at room temperature. 5 µL propidium iodide and 400 µL of phosphate-buffered solution (PBS; P1022, Solarbio, Beijing, China) were added to the cell suspension. Finally, the cells were detected and analyzed by BD FACSAria™ Fusion flow cytometer and BD FACSDiva™ software (BD Biosicences, San Diego, CA, USA), respectively.

Wound Healing Assay

When the HCT116 and SW480 cells in 6-well plates reached nearly 100% confluence, a scratch was made across cell monolayer using a pipette tip. After 48-h incubation in serum-free medium, the gap closure was visualized using a microscope (×100 magnification; CX43, Olympus, Tokyo, Japan). The cell migration rate was determined using formula in the following:

Cell migration rate (%) = (Scratch width at 0 h – Scratch width at 24 h)/Scratch width at 0 h × 100

The data in the experimental groups were normalized to the data in the blank group.

Transwell Assay

Transference of HCT116 and SW480 cells to the upper Transwell chamber (8 µm; 3422, Corning, Inc., Corning, NY, USA) in a 24-well plate was performed where 200 µL serum-free medium was added and Matrigel matrix (354234, Corning, Inc., USA) was coated. Meanwhile, the lower Transwell chamber contained 700 µL serum-supplemented medium (chemoattractant). Following a 48-h incubation, only invasive cells were fixed with 4% paraformaldehyde (MM1504, Shanghai Maokang Biotechnology Co., Ltd., Shanghai, China) at 4 °C for 10 min and stained with crystal violet for 30 min. Finally, the invasive cells were observed under a CX43 microscope (×250 magnification). The cell invasion rate was calculated using the formula in the following:

Cell invasion rate (%) = (Invasive cell number at 24 h – Invasive cell number at 0 h)/Total cell number × 100

The data in the experimental groups were normalized to the data in the blank group.

Western Blotting

Total protein isolation (from HCT116 and SW480 cells) and protein concentration quantification were accomplished using RIPA Lysis Buffer (R0020, Solarbio, Beijing, China) and bicinchoninic acid (BCA) protein assay kit (23225, Thermo Fisher Scientific, Waltham, MA, USA), respectively. Isolated proteins (20 µg) were separated by 6–8% sodium dodecyl sulfate polyacrylamide gel electrophoresis (P0012A, Beyotime, Shanghai, China) and subsequently transferred from gel onto polyvinylidene fluoride membranes (FFP24, Beyotime, Shanghai, China). The membranes were then subjected to blocking using 5% bovine serum albumin (SW3015, Solarbio, Beijing, China) in Tris-buffered saline containing Tween-20 (ST671, Beyotime, Shanghai, China) at room temperature for 2 h. Next, the membranes were incubated with primary antibodies including SLIT3 (1:1000, 168 kDa, ab151724), E-cadherin (E-Cad; 1:1000, 135 kDa, #14472), N-cadherin (N-Cad; 1:1000, 140 kDa, #14215), Snail (1:500, 68 kDa, ab53519), cyclin D3 (1:100, 33 kDa, ab183338), glyceraldehyde-3-phosphate dehydrogenase (GAPDH) (1:10000, 36 kDa, ab8245) at 4 °C overnight. Afterward, the membranes were subjected to incubation with secondary antibodies, either horseradish peroxidase-conjugated goat anti-rabbit IgG (1:2000, ab205718) or rabbit anti-mouse IgG (1:2000, ab6728) at room temperature for 2 h. Immunoblot signals were visualized by ECL Plus kit (P0018S, Beyotime, Shanghai, China) on an imaging system (5200 Multi, Tanon, Shanghai, China), and the gray scale value was calculated using ImageJ software version 1.8.0 (National Institutes of Health, Bethesda, MD, USA). The above antibodies were available from Abcam (Cambridge, UK), except for E-Cad and N-Cad, which were procured from Cell SignalingTechnology (Beverly, MA, USA).

Mouse Tumor Xenograft

Balb/c nude mice (male, 20 ± 2 g, 6-week-old, n = 6) obtained from Vital River (Beijing, China) were bred in cages (22 ± 2 °C, 50 ± 10% humidity, 12-h circadian rhythm), and divided into negative control (NC) and si*BARD1* groups (n = 3/group), in which the mice underwent subcutaneous injection of si*NC*- or si*BARD1*-transfected HCT116 cells (5×10^6) in the flank regions [17], respectively. The total tumor volumes were evaluated at days 5, 10, 15, 20, 25 and 30 and calculated using the formula in the following:

Tumor volume (mm^3) = Length (L) × width $(W)^2/2$

Finally, 2% pentobarbital sodium (50 mg/kg; P3761, Haoran Biological Technology, Shanghai, China)-anesthetized mice were euthanized by cervical dislocation, after which the tumors were acquired, photographed, and weighed.

Immunohistochemistry

Tumors were fixed by 4% paraformaldehyde at room temperature for 20 min, followed by dehydration with alcohol (64-17-5, Sigma Aldrich, Darmstadt, Germany) and permeabilization with xylene (X112054, Aladdin, Shanghai, China). Thereafter, paraffin-embedded (YA0012, Solarbio, Beijing, China) sections, with a thickness of 6 µm each, were acquired, After being treated with xylene and alcohol, the sections were permeabilized with 0.1% Triton X-100 (P1080, Solarbio, Beijing, China) for 5 min, and immersed in Citrate Antigen Retrieval Solution (P0081, Beyotime, Shanghai, China) pre-heated at 95–100 °C for 20 min. Next, the sections were blocked with goat serum (C0265, Beyotime, Shanghai, China), and successively incubated with primary antibody targeting cy-

Journal of
BIOLOGICAL REGULATORS
and Homeostatic Agents

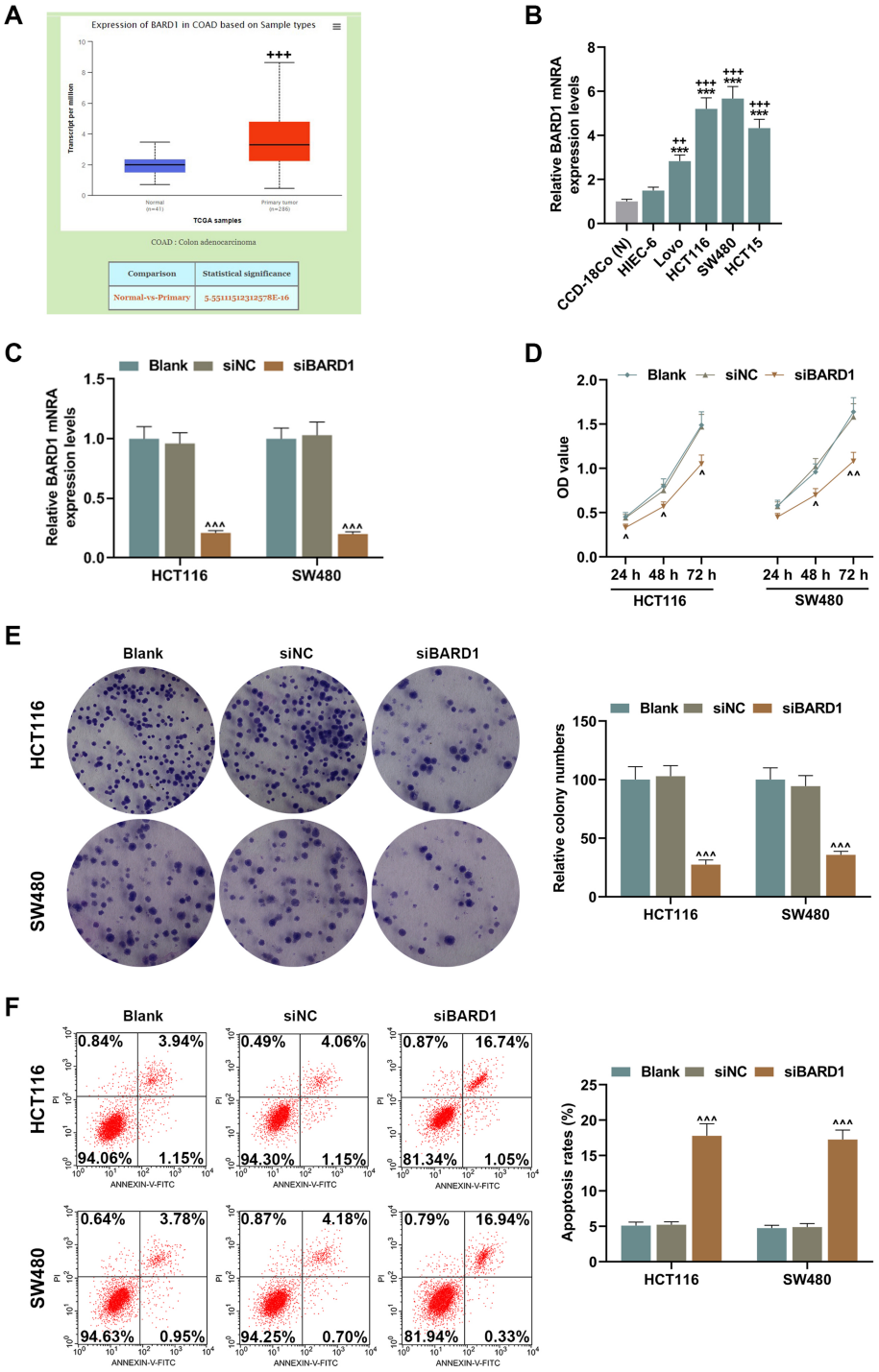

Fig. 1. *BARD1* expression in CRC cells, and effects of si*BARD1* on CRC cell viability, proliferation, and apoptosis. (A) *BARD1* expression in COAD (source: data retrieved from UALCAN database). (B) *BARD1* expression in HIEC-6, Lovo, HCT116, SW480, HCT15, and CCD-18Co cells (detected by qRT-PCR, using *GAPDH* as the internal control). (C) *BARD1* expression in HCT116 and SW480 cells transfected with si*BARD1* (detected by qRT-PCR, using *GAPDH* as the internal control). (D–F) Viability (D), proliferation (E) and apoptosis (F) of HCT116 and SW480 cells transfected with si*BARD1* detected by cell counting kit-8 assay, colony formation assay, and flow cytometry. n = 3. $^{++}p < 0.01$, $^{+++}p < 0.001$, vs. Normal or HIEC-6; $^{***}p < 0.001$, vs. CCD-18Co (N); $^{\wedge}p < 0.05$, $^{\wedge\wedge}p < 0.01$, $^{\wedge\wedge\wedge}p < 0.001$, vs. siNC. Abbreviations: *BARD1*, BRCA1 associated RING domain 1; CRC, colorectal cancer; si*BARD1*, small interfering RNA targeting *BARD1*; COAD, colon adenocarcinoma; UALCAN, University of Alabama at Birmingham Cancer Data Analysis Portal; qRT-PCR, quantitative real-time reverse transcription polymerase chain reaction; *GAPDH*, glyceraldehyde-3-phosphate dehydrogenase; siNC, small interfering RNA of negative control.

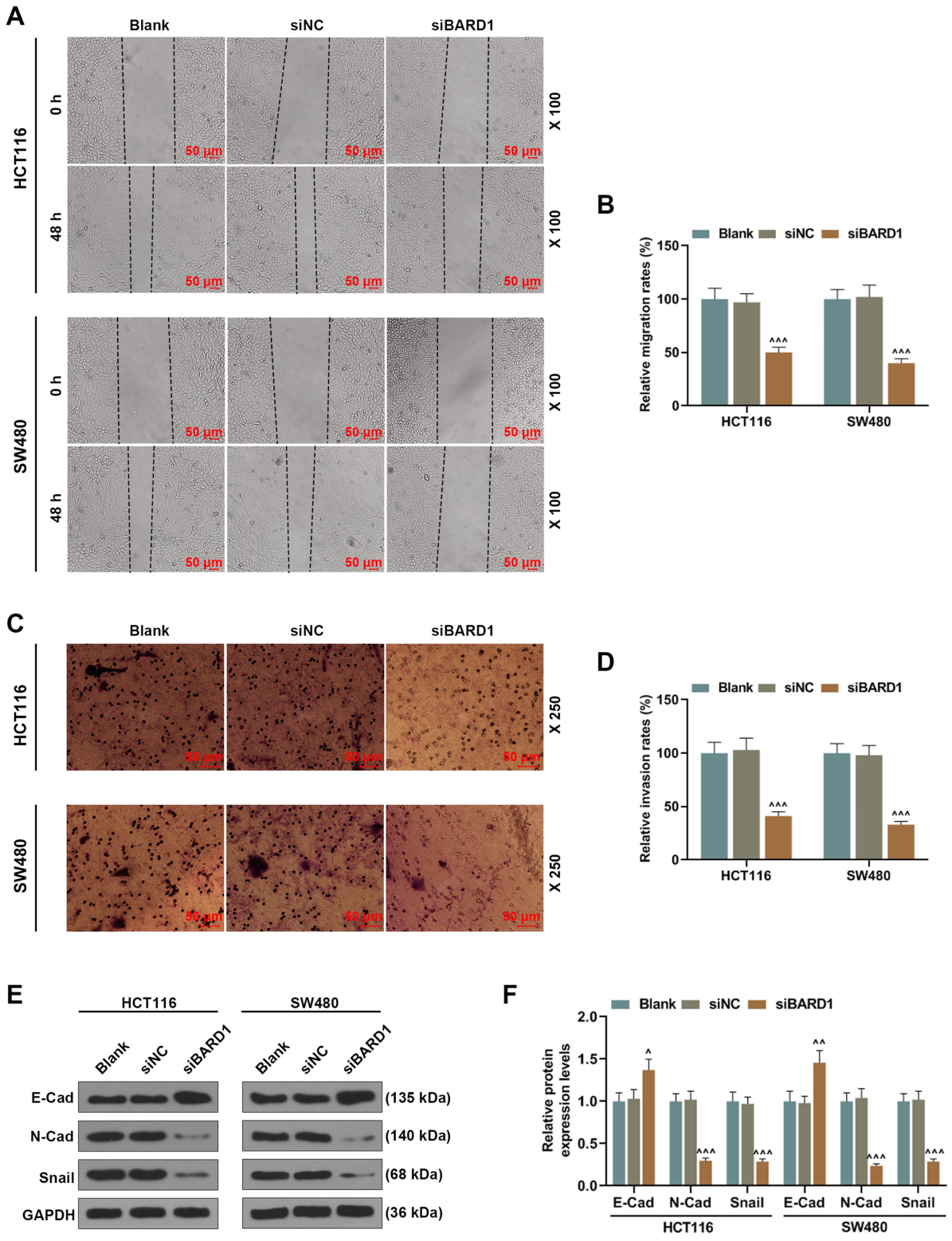

Fig. 2. Effects of si*BARD1* transfection on migration, invasion, and EMT activation in CRC cells. (A–F) Migration ((A,B), ×100 magnification, scale bar: 50 μm), invasion ((C,D), ×250 magnification, scale bar: 50 μm), and expression of EMT-associated proteins such as E-Cad, N-Cad, and Snail (E,F) in HCT116 and SW480 cells after the interference of si*BARD1*. GAPDH was employed as the internal control. n = 3. $^{\wedge}p < 0.05$, $^{\wedge\wedge}p < 0.01$, $^{\wedge\wedge\wedge}p < 0.001$, vs. siNC. Abbreviations: *BARD1*, BRCA1 associated RING domain 1; si*BARD1*, small interfering RNA targeting *BARD1*; CRC, colorectal cancer; EMT, epithelial mesenchymal transition; E-Cad, E-cadherin; N-Cad, N-cadherin; GAPDH, glyceraldehyde-3-phosphate dehydrogenase; siNC, small interfering RNA of negative control.

Journal of
BIOLOGICAL REGULATORS
and Homeostatic Agents

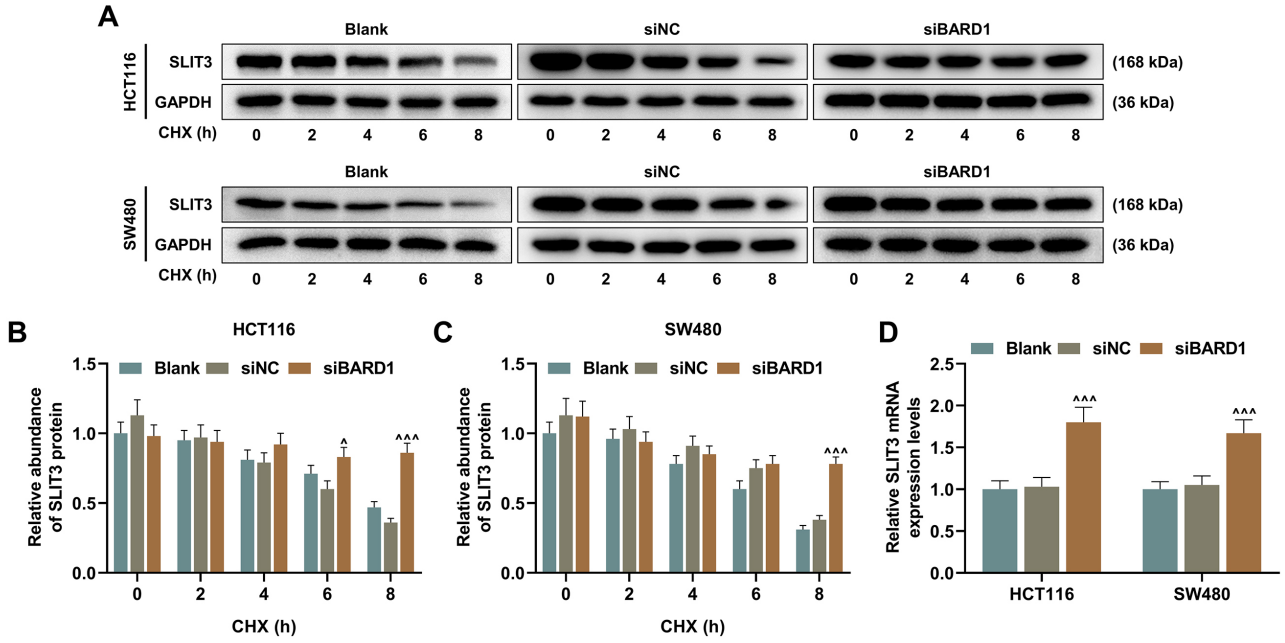

Fig. 3. Effects of si*BARD1* on *SLIT3* degradation. (A–D) *SLIT3* protein abundance detected by western blotting (A–C) and mRNA expression level detected by qRT-PCR (D) in HCT116 and SW480 cells experiencing si*BARD1* interference and treatment of 0.2 mg/mL CHX (an inhibitor of protein synthesis) for 0, 2, 4, 6, and 8 h at 37 °C. GAPDH was treated as the internal control. n = 3. $^{\wedge}p < 0.05$, $^{\wedge\wedge\wedge}p < 0.001$, vs. siNC. Abbreviations: *BARD1*, BRCA1 associated RING domain 1; si*BARD1*, small interfering RNA targeting *BARD1*; *SLIT3*, slit guidance ligand 3; CHX, cycloheximide; GAPDH, glyceraldehyde-3-phosphate dehydrogenase.

clin D3 (ab289546, 1:5000, Abcam, Cambridge, UK) at 4 °C overnight, and secondary antibodies against mouse IgG (VC001-125, 1:1000, Novus Biologicals, Littelton, CO, USA) at 37 °C for 1 h. Later, the sections were incubated with 3,3′-diaminobenzidine tetrahydrochloride (DAB; G1212, Servicebio, Wuhan, China) for 10 min, and counterstained with hematoxylin (C0107, Beyotime, Shanghai, China) for 2 min. Finally, the sections were dehydrated, cleared with xylene, and sealed with neutral gum (96949-21-2, Solarbio, Beijing, China). The slides were observed under CX31 microscope (×100 magnification; Olympus, Tokyo, Japan).

Quantitative Real-Time Reverse Transcription Polymerase Chain Reaction

Total RNA extraction (tumor tissues and HCT116/SW480 cells) and concentration detection were accomplished using TRIzol (15596026) and ND-2000 spectrophotometer (Thermo Fisher Scientific, Waltham, MA, USA), respectively. cDNA synthesis was performed using primeScript™ RT reagent kit (RR037A, TaKaRa, Beijing, China). Afterwards, PCR was conducted using SYBR Green qPCR mix (D7260, Beyotime, Shanghai, China) at designated thermal cycling conditions: 95 °C (2 min), and 40 cycles of 95 °C (15 s for each cycle) and 60 °C (15 s). Relative gene expression was calculated by $2^{-\Delta\Delta Ct}$ method [19], using *GAPDH* as the internal control.

All primer sequences (5′–3′) are listed below: *BARD1* (human): forward, GAGCCTGTGTGTTTAGGAGGA, reverse, ACTTCGAGGGCTAAACCACA; *SLIT3* (human): forward, TGACATTTCCAGCGTTCCTGA, reverse, GAGTACTTTGCACTGGAAGCG; cyclin D3 (human): forward, CTGTGCATCTACACCGACCA, reverse, AGAGGGCCAAAAAGGTCTGG; glyceraldehyde-3-phosphate dehydrogenase (*GAPDH*) (human): forward, CAGCCTCAAGATCATCAGCA, reverse, TGTGGTCATGAGTCCTTCCA.

Statistical Analyses

Analyses of all data were performed on GraphPad Prism 8.0 (GraphPad Software Inc., San Diego, CA, USA). Quantitative data are expressed as mean ± standard deviation. Two-group or multi-group data were compared using independent samples *t* test or one-way analysis of variance, followed by the post-hoc Tukey test. *p*-value < 0.05 was perceived to be of statistical significance.

Results

BARD1 Expression was Upregulated in CRC Cells

According to the gene expression data of colon adenocarcinoma (COAD) retrieved from UALCAN database and TIMER database, we found that *BARD1* expression is upregulated in CRC (Fig. 1A and **Supplementary Fig. 1**). In addition, *BARD1* was correlated with cell cycle and DNA

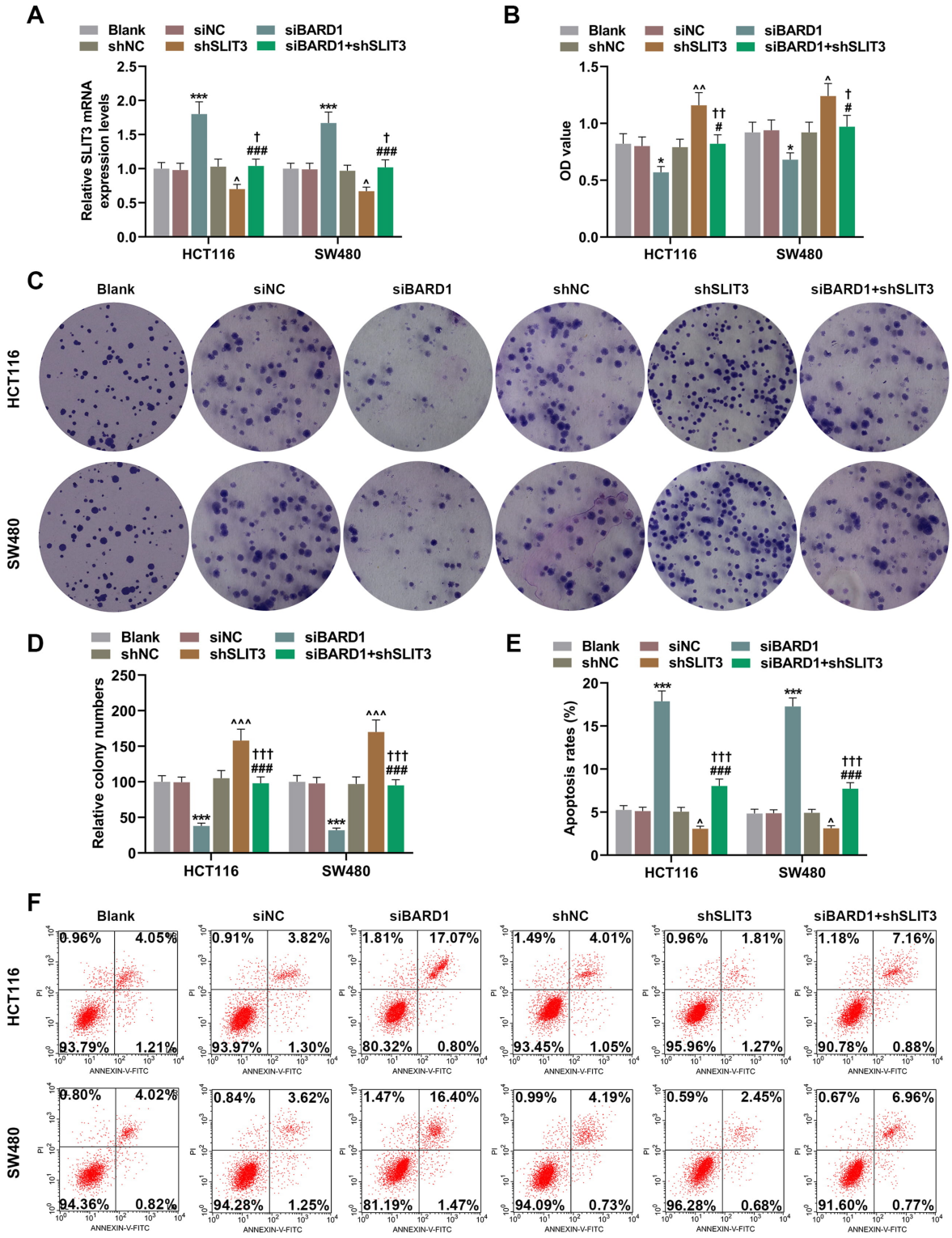

Fig. 4. Effects of si*BARD1* and sh*SLIT3* on *SLIT3* expression, viability, proliferation, and apoptosis of CRC cells. (A–F) *SLIT3* expression (A), viability (B), proliferation (C,D), and apoptosis (E,F) of CRC cells transfected with si*BARD1* and sh*SLIT3*. n = 3. $^{*}p < 0.05$, $^{***}p < 0.001$, vs. siNC; $^{\wedge}p < 0.05$, $^{\wedge\wedge}p < 0.01$, $^{\wedge\wedge\wedge}p < 0.001$, vs. shNC; $^{\dagger}p < 0.05$, $^{\dagger\dagger}p < 0.01$, $^{\dagger\dagger\dagger}p < 0.001$, vs. sh*SLIT3*; $^{\#}p < 0.05$, $^{\#\#\#}p < 0.001$, vs. si*BARD1*. Abbreviations: *BARD1*, BRCA1 associated RING domain 1; si*BARD1*, small interfering RNA targeting *BARD1*; *SLIT3*, slit guidance ligand 3; sh*SLIT3*, short hairpin RNA against *SLIT3*; shNC, short hairpin RNA of negative control; CRC, colorectal cancer; qRT-PCR, quantitative real-time reverse transcription polymerase chain reaction; *GAPDH*, glyceraldehyde-3-phosphate dehydrogenase.

Journal of
BIOLOGICAL REGULATORS
and Homeostatic Agents

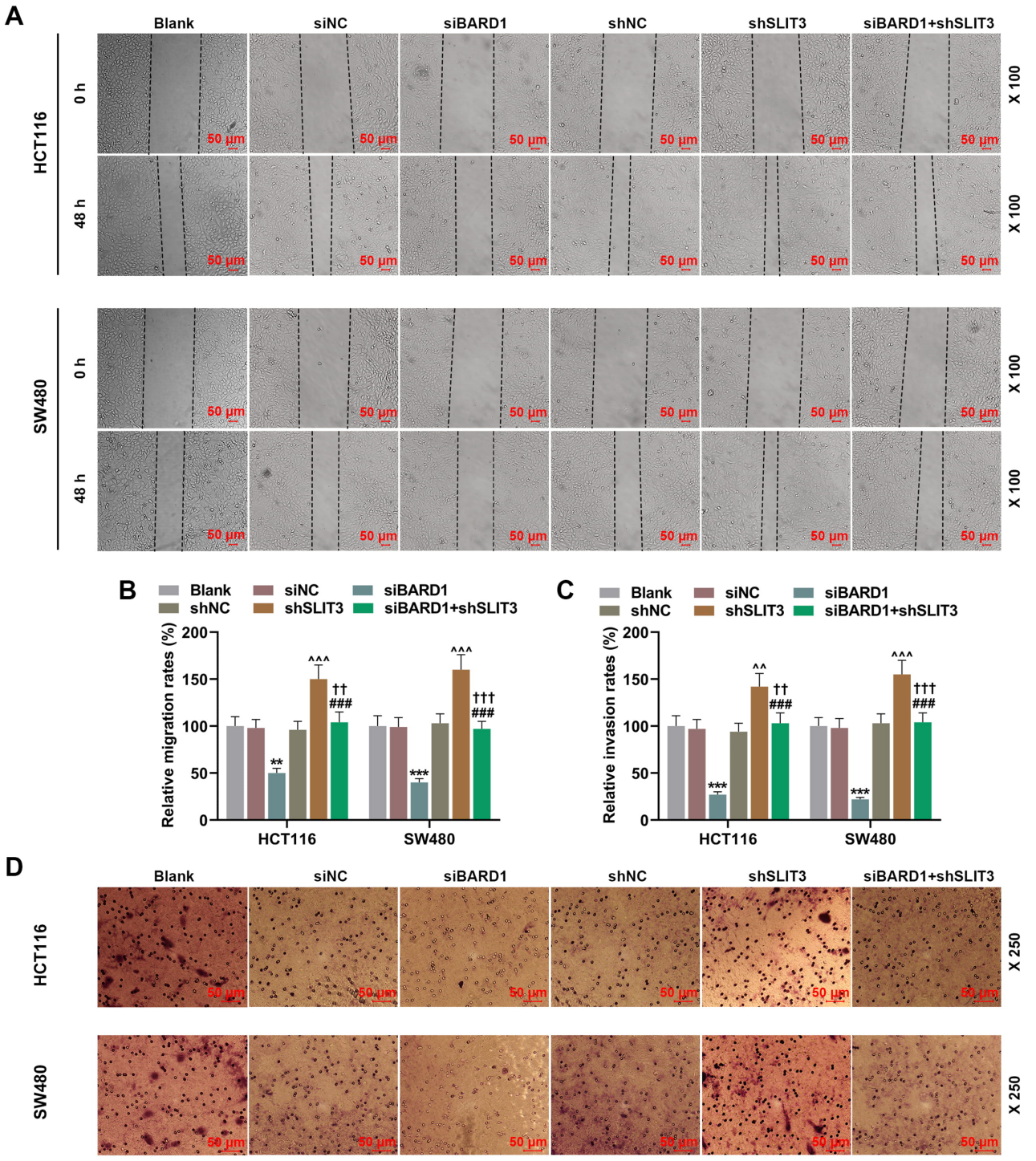

Fig. 5. Effects of si*BARD1* and sh*SLIT3* on migration and invasiveness of CRC cells. (A–D) Migration ((A,B), ×100 magnification, scale bar: 50 μm) and invasiveness ((C,D), ×250 magnification, scale bar: 50 μm) of CRC cells transfected with si*BARD1* and sh*SLIT3*. n = 3. $^{**}p < 0.01$, $^{***}p < 0.001$, vs. siNC; $^{\wedge\wedge}p < 0.01$, $^{\wedge\wedge\wedge}p < 0.001$, vs. shNC; $^{\dagger\dagger}p < 0.01$, $^{\dagger\dagger\dagger}p < 0.001$, vs. sh*SLIT3*; $^{\#\#\#}p < 0.001$, vs. si*BARD1*. Abbreviations: *BARD1*, BRCA1 associated RING domain 1; si*BARD1*, small interfering RNA targeting *BARD1*; *SLIT3*, slit guidance ligand 3; sh*SLIT3*, short hairpin RNA against *SLIT3*; shNC, short hairpin RNA of negative control; CRC, colorectal cancer.

replication, based on GSEA (**Supplementary Figs. 2,3**). Besides, higher level of *BARD1* expression was detected in Lovo, HCT116, SW480, and HCT15 cells relative to CCD-18Co and HIEC-6 cells (Fig. 1B, $p < 0.01$). By virtue of the highest *BARD1* expression detected in HCT116 and SW480 cells, these two cell lines were selected to conduct subsequent experiments.

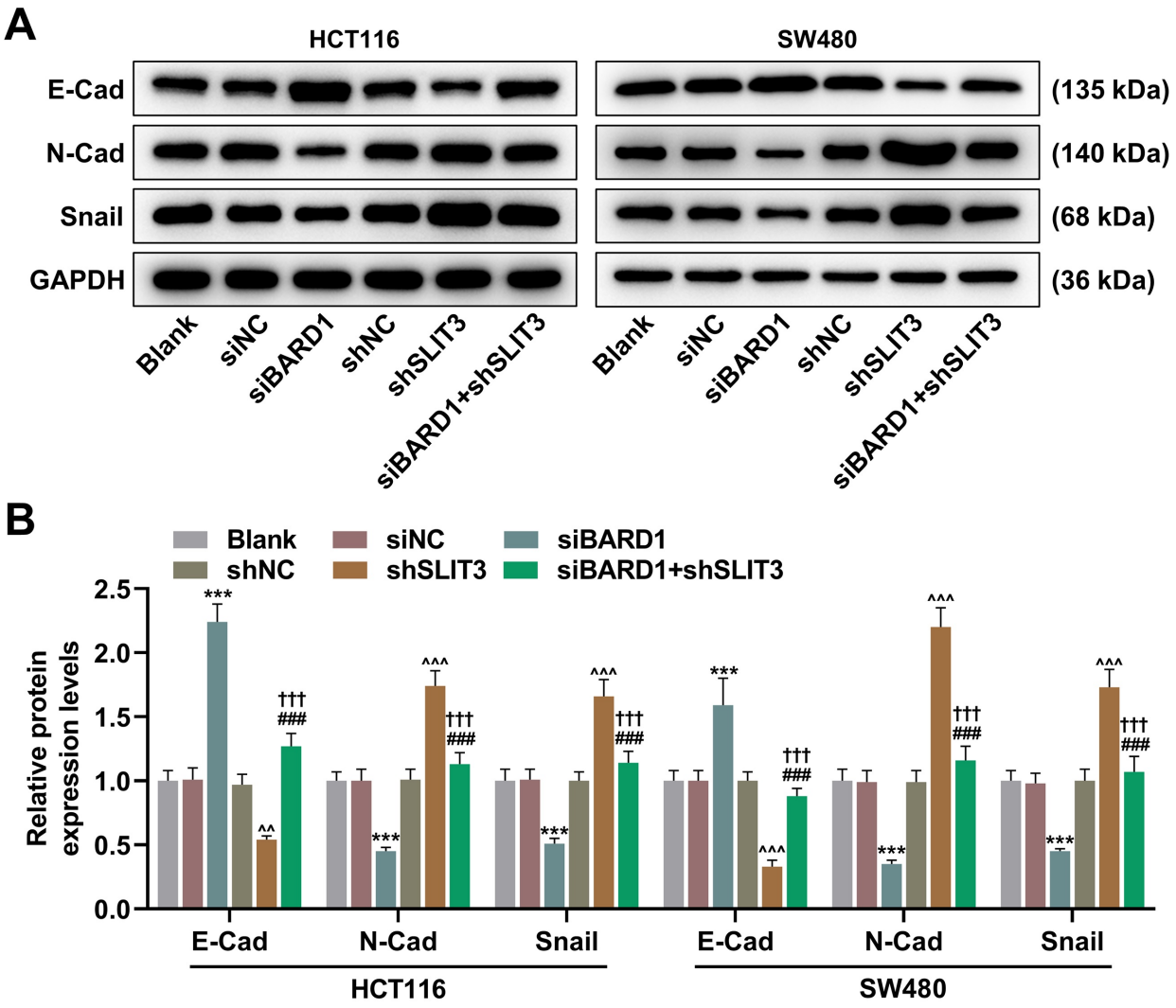

Fig. 6. Effects of si*BARD1* and sh*SLIT3* on EMT activation in CRC cells. (A,B) Expression of EMT-associated proteins such as E-Cad, N-Cad, and Snail in CRC cells transfected with si*BARD1* and sh*SLIT3*: western blot of EMT-associated proteins, with GAPDH serving as internal control. n = 3. ***$p < 0.001$, vs. siNC; $^{\dagger\dagger\dagger}p < 0.001$, vs. sh*SLIT3*; $^{\wedge\wedge}p < 0.01$, $^{\wedge\wedge\wedge}p < 0.001$, vs. shNC; $^{\#\#\#}p < 0.001$, vs. si*BARD1*. Abbreviations: *BARD1*, BRCA1 associated RING domain 1; si*BARD1*, small interfering RNA targeting *BARD1*; *SLIT3*, slit guidance ligand 3; sh*SLIT3*, short hairpin RNA against *SLIT3*; shNC, short hairpin RNA of negative control; CRC, colorectal cancer; GAPDH, glyceraldehyde-3-phosphate dehydrogenase.

SiBARD1 Suppressed Malignant Phenotype and Epithelial Mesenchymal Transition in CRC Cells

Si*BARD1* was successfully transfected into HCT116 and SW480 cells, as confirmed by reduced *BARD1* expression in cells (Fig. 1C, $p < 0.001$). The subsequent CCK-8 (Fig. 1D), colony formation (Fig. 1E), flow cytometry (Fig. 1F), wound healing (Fig. 2A,B), and Transwell (Fig. 2C,D) assays revealed reduced viability, proliferation, migration and invasion, and an increase of apoptosis following the transfection of si*BARD1* into HCT116 and SW480 cells ($p < 0.05$). These results preliminarily confirmed that si*BARD1* could inhibit malignant phenotype of CRC cells. Then, we measured the expression of epithelial mesenchymal transition (EMT)-associated protein (E-Cad, N-Cad, and Snail) in HCT116 and SW480 cells, further shedding light on the influences of *BARD1* deletion on CRC cells. Fig. 2E,F revealed si*BARD1* elevated E-Cad level while diminishing N-Cad and Snail levels in HCT116 and SW480 cells ($p < 0.05$), confirming that si*BARD1* suppressed the activation of EMT.

SiBARD1 Suppressed the Degradation of SLIT3

To verify the effects of *BARD1* on *SLIT3* degradation, HCT116 and SW480 cells were treated with 0.2 mg/mL CHX for 0, 2, 4, 6, and 8 h. As displayed in Fig. 3A–C, the abundance of *SLIT3* protein was obviously augmented after the deletion of *BARD1* in HCT116 and SW480 cells, hinting at the enhanced stability of *SLIT3* in *BARD1*-deleted

Journal of
BIOLOGICAL REGULATORS
and Homeostatic Agents

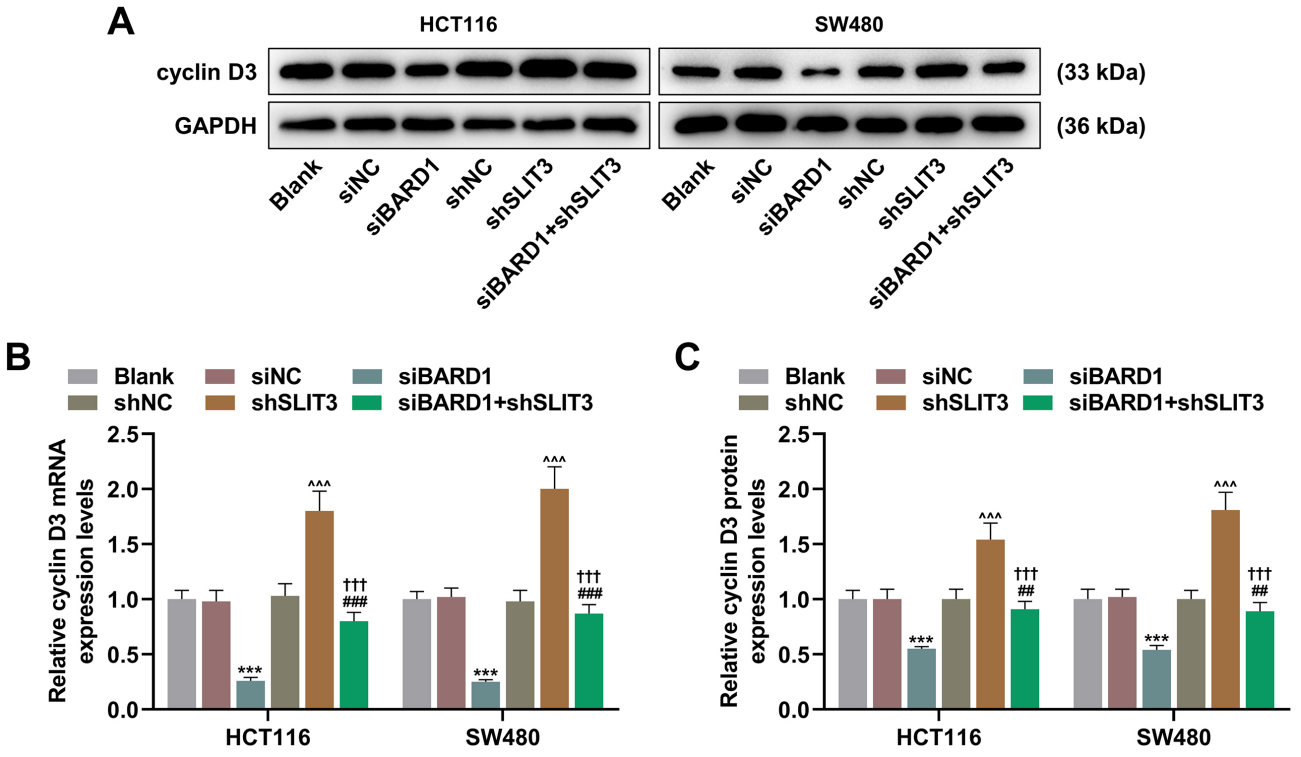

Fig. 7. Effects of si*BARD1* and sh*SLIT3* on cyclin D3 expression in CRC cells transfected with si*BARD1* and sh*SLIT3*. (A) Western blot of cyclin D3 in CRC cells. (B) Expression levels of cyclin D3 mRNA in CRC cells. (C) Relative cyclin D3 protein expression levels in CRC cells. GAPDH was treated as the internal control. n = 3. $^{***}p < 0.001$, vs. siNC; $^{\dagger\dagger\dagger}p < 0.001$, vs. sh*SLIT3*; $^{\wedge\wedge\wedge}p < 0.001$, vs. shNC; $^{\#\#}p < 0.01$, $^{\#\#\#}p < 0.001$, vs. si*BARD1*. Abbreviations: *BARD1*, BRCA1 associated RING domain 1; si*BARD1*, small interfering RNA targeting *BARD1*; *SLIT3*, slit guidance ligand 3; sh*SLIT3*, short hairpin RNA against *SLIT3*; shNC, short hairpin RNA of negative control; CRC, colorectal cancer; qRT-PCR, quantitative real-time reverse transcription polymerase chain reaction; GAPDH, glyceraldehyde-3-phosphate dehydrogenase.

CRC cells. Also, *SLIT3* expression was noticed to be up-regulated after the transfection of si*BARD1* in HCT116 and SW480 cells (Fig. 3D, $p < 0.001$).

ShSLIT3 Led to Malignant Phenotype, EMT Activation, and Elevated Cyclin D3 Level in CRC Cells, which Were Reversable by SiBARD1

To further explore the effects of *SLIT3* on CRC cells and its interaction with *BARD1*, sh*SLIT3* was transfected into HCT116 and SW480 cells, resulting in reduced *SLIT3* level (Fig. 4A, $p < 0.05$). From this study, we learned that the transfection of sh*SLIT3* and si*BARD1* exerted mutually antagonistic cellular effects (Fig. 4A, $p < 0.001$, $p < 0.05$).

According to Fig. 4B–F, Fig. 5A–D and Fig. 6A,B, sh*SLIT3* transfection led to increased viability, proliferation, migration, and invasion; downregulation of E-Cad; and upregulation of N-Cad and Snail in HCT116 and SW480 cells ($p < 0.05$), but apoptosis was only marginally reduced. As expected, co-transfection of sh*SLIT3* and si*BARD1* resulted in mutually neutralization of these cellular effects, including apoptosis (Fig. 4B-6B, $p < 0.05$). Besides, it was evident that si*BARD1* suppressed while sh*SLIT3* enhanced cyclin D3 mRNA or protein expression level in HCT116 and SW480 cells, and sh*SLIT3* and si*BARD1* can mutually attenuate their impacts (Fig. 7A–C, $p < 0.001$).

SiBARD1 Hindered Tumor Growth, Reduced Cyclin D3 Level, and Promoted SLIT3 Expression in vivo

Furthermore, we focused on exploring the effects of *BARD1* deletion *in vivo* following tumor formation in nude mice injected with si*BARD1*/siNC-transfected cells. In accordance with the results in Fig. 8A–C, si*BARD1* reduced the tumor volume and weight ($p < 0.001$), suggesting that *BARD1* deletion suppressed the tumor growth *in vivo*. Meanwhile, si*BARD1* was found to diminish cyclin D3 level and augment *SLIT3* expression *in vivo* (Fig. 8D–F, $p < 0.001$).

Discussion

A more profound understanding on how *BARD1* impacts malignant behaviors of CRC cells and the potential underlying mechanisms will help us gain clarity about

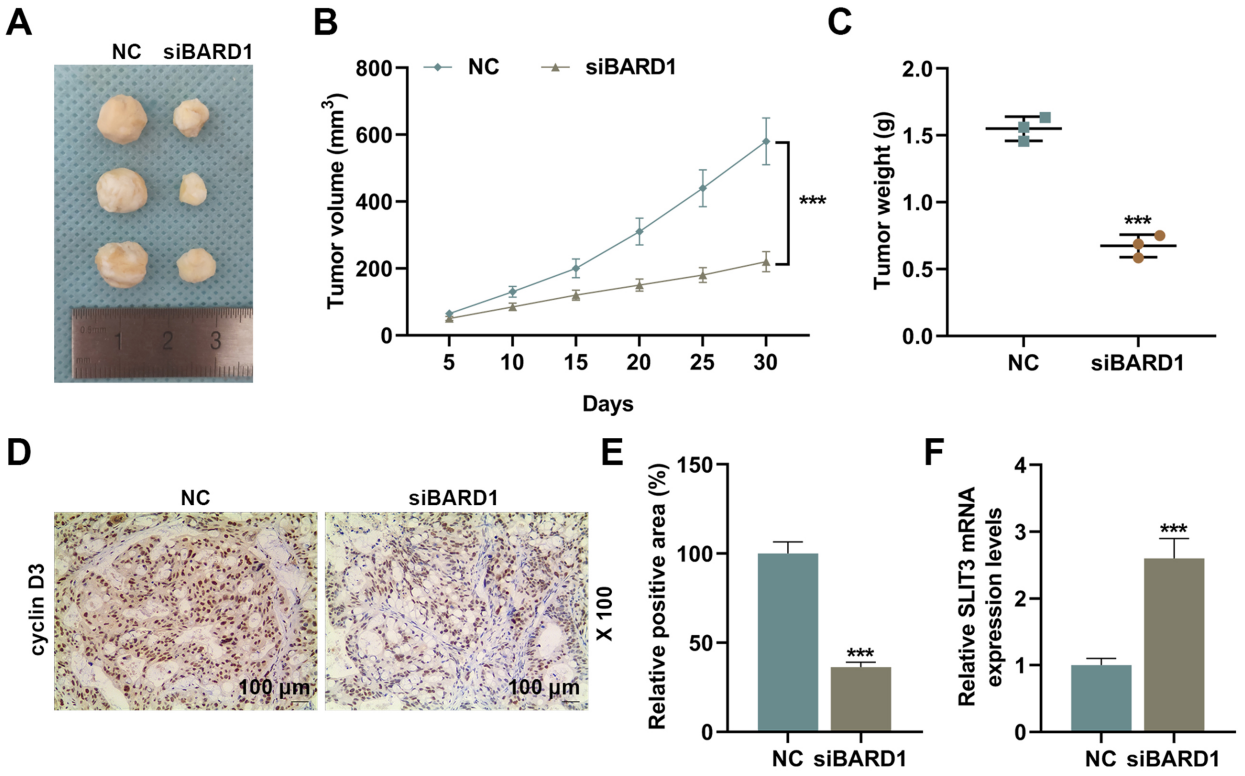

Fig. 8. Effects of si*BARD1* on tumor growth and expression of cyclin D3 protein and *SLIT3* mRNA *in vivo*. (A) The tumors obtained from mice in the NC and siBARD1 groups. (B) Changes in tumor volume after 5, 10, 15, 20, 25, 30 days of the treatment involving subcutaneous injection of si*BARD1*-transfected HCT116 cells (5×10^6) into Balb/c nude mice. (C) Tumor weight after sacrifice of mice. (D) Immunohistochemical staining of cyclin D3; the brown and blue colorations are the results of DAB and hematoxylin staining, respectively (×100 magnification, scale bar: 100 μm). (E) The positive area of cyclin D3 in mouse tumor tissues of NC and siBARD1 groups. (F) *SLIT3* expression, as detected by qRT-PCR using *GAPDH* as the internal control. n = 3. ***$p < 0.001$, vs. NC. Abbreviations: *BARD1*, BRCA1 associated RING domain 1; si*BARD1*, small interfering RNA targeting *BARD1*; *SLIT3*, slit guidance ligand 3; DAB, 3,3′-diaminobenzidine tetrahydrochloride; qRT-PCR, quantitative real-time reverse transcription polymerase chain reaction; *GAPDH*, glyceraldehyde-3-phosphate dehydrogenase.

the pathogenesis of CRC, inspiring the discovery of new molecular targets and offering a valid basis for early clinical diagnosis and treatment of CRC. Both the UALCAN database and our qRT-PCR results confirmed the upregulation of *BARD1* expression in CRC. Our *in vitro* experiments revealed that *BARD1* deletion significantly suppressed malignant phenotypes and EMT of CRC cells. Combined with the effect of *BARD1* consistently confirmed on CRC tumor growth *in vivo,* these findings corroborate *BARD1* as a potential molecular target for CRC therapy.

The involvement of *BARD1* in cancers has generated considerable research interest over the past decade. In light of published researches, *BARD1* functions as both tumor suppressor gene and oncogene in the context of tumorigenesis [7,8]. Deficient *BARD1* expression is a vital factor for tumorigenesis in breast cancer [20]. Nevertheless, from the angle of different tumor type, CRC has been verified to possess upregulated *BARD1* expression, and the clinical prognosis of CRC seems to be associated with *BARD1* [13]. While *BARD1* modulates the predisposition of an individual toward developing CRC, *BARD1* variants have been found to participate in the occurrence of the early onset of CRC [21]. Also, it has been acknowledged that invasive phenotype of colon cancer cells is related to the *BARD1β* (a *BARD1* splice variant) [22]. Herein, the results showed that *BARD1* deletion restrained CRC cell malignant phenotype, implying the role of *BARD1* in promoting the aggressiveness and progression of CRC. Besides, aberrant activation of EMT is instrumental in cancer cell metastasis [23], strengthening the resistance to immunotherapy as well as immune suppression [24]. E-Cad, N-Cad, and Snail are the EMT-associated proteins [25,26]. It should be mentioned that *BARD1* has a great impact on EMT [27]. Accordingly, we further demonstrated that si*BARD1* suppressed EMT in CRC cells via E-Cad upregulation and downregulation of N-Cad and Snail. Taken together, these findings portray an apparent mechanism underlying the suppression of malignant phenotype of CRC cells following *BARD1* deletion via reversal of EMT process.

Journal of
BIOLOGICAL REGULATORS
and Homeostatic Agents

Compelling evidence has highlighted that *BRCA1*/*BARD1* complex can regulate expression of some proteins [14]. Based on the Ubibrowser database, SLIT3 is one of the BARD1 substrates. The current set of results suggested that si*BARD1* suppressed the degradation of *SLIT3*. The downregulation of *SLIT3* in CRC has been reported [15], and the involvement of *SLIT3* in the progression of bladder [28], thyroid [29], and gastric [30] cancers has been verified. Likewise, it has been validated that *SLIT3* is expressed at low levels in HCC tumor tissues and other cancers, denoting *SLIT3* as a promising target for HCC treatment [17]. Yet the role of *SLIT3* in CRC remains poorly understood. We additionally confirmed that *BARD1* deletion could suppress the malignant phenotype of CRC cells by blocking *SLIT3* degradation, and that *SLIT3* participated in the suppression of EMT mediated by *BARD1* deletion. Moreover, it is worth mentioning that chemoresistance in HCC is induced by *SLIT3* repression, which is achieved by upregulating cyclin D3 level [17], and that elevated cyclin D3 can facilitate the progression of CRC [18]. Hence, we evaluated cyclin D3 expression following the gene expression interference mediated by si*BARD1* and sh*SLIT3* in CRC cells. In accordance with prior findings, *SLIT3* knockdown can elevate cyclin D3 expression while *BARD1* deletion leads to an opposite effect, which has a bearing on CRC progression through regulation of *SLIT3* expression.

Further, the effects of *BARD1* deletion were also verified in tumor xenograft performed in animal models. From the results obtained in this study, the tumor volume and weight were all apparently diminished following the intervention using si*BARD1*, reflecting the effect of *BARD1* deletion on tumor growth suppression. As for the cyclin D3 expression, immunohistochemistry data showed a reduced expression of cyclin D3 after the *BARD1* deletion, which was in accordance with the results obtained from *in vitro* experiment. Additionally, we also elucidated the regulatory impact of *BARD1* deletion on *SLIT3* expression, which was expressed at high levels *in vivo* after the deletion of *BARD1*. Nonetheless, this study is constrained by certain limitations. For example, whether *BARD1* can directly target *SLIT3* in CRC cells remains unknown and was not explored in this study.

Conclusion

In conclusion, *BARD1* deletion hampers CRC progression by modulating the *SLIT3*/cyclin D3 axis. Accordingly, *BARD1* holds promise as a new biomarker or a target of molecular therapy for CRC.

Availability of Data and Materials

The analyzed data sets generated during the study are available from the corresponding author on reasonable request.

Author Contributions

Substantial contributions to conception and design: YWZ, SFY. Data acquisition, data analysis and interpretation: YYL, BC, YJW, ZLZ. Drafting the article or critically revising it for important intellectual content: All authors. Final approval of the version to be published: All authors. Agreement to be accountable for all aspects of the work in ensuring that questions related to the accuracy or integrity of the work are appropriately investigated and resolved: All authors.

Ethics Approval and Consent to Participate

In compliance with the guidelines of the China Council on Animal Care and Use, all animal experiments in this study were performed. The experimental protocol received approval from the Institutional Animal Care and Use Committee of Zhejiang Center of Laboratory Animals (No. ZJCLA-IACUC-20010231).

Acknowledgment

Not applicable.

Funding

This work was supported by the Second Batch of Scientific and Technological Innovation Team of Lishui Digestive Endoscopy Clinical Research Scientific and Technological Innovation Team [2018cxtd05].

Conflict of Interest

The authors declare no conflict of interest.

Supplementary Material

Supplementary material associated with this article can be found, in the online version, at https://doi.org/10.23812/j.biol.regul.homeost.agents.20243805.334.

References

[1] Ciardiello F, Ciardiello D, Martini G, Napolitano S, Tabernero J, Cervantes A. Clinical management of metastatic colorectal cancer in the era of precision medicine. CA: a Cancer Journal for Clinicians. 2022; 72: 372–401.

[2] Kim EK, Song MJ, Jung Y, Lee WS, Jang HH. Proteomic Analysis of Primary Colon Cancer and Synchronous Solitary Liver Metastasis. Cancer Genomics & Proteomics. 2019; 16: 583–592.

[3] Kumamoto K, Nakachi Y, Mizuno Y, Yokoyama M, Ishibashi K, Kosugi C, *et al*. Expressions of 10 genes as candidate predictors of recurrence in stage III colon cancer patients receiving adjuvant oxaliplatin-based chemotherapy. Oncology Letters. 2019; 18: 1388–1394.

[4] Zheng Y, Meng L, Liu H, Sun L, Nie Y, Wu Q, *et al*. Let food be thy medicine: the role of diet in colorectal cancer: a narrative

review. Journal of Gastrointestinal Oncology. 2022; 13: 2020–2032.

[5] Yang Z, Wu G, Zhang X, Gao J, Meng C, Liu Y, *et al*. Current progress and future perspectives of neoadjuvant anti-PD-1/PD-L1 therapy for colorectal cancer. Frontiers in Immunology. 2022; 13: 1001444.

[6] Yang Z, Deng W, Zhang X, An Y, Liu Y, Yao H, *et al*. Opportunities and Challenges of Nanoparticles in Digestive Tumours as Anti-Angiogenic Therapies. Frontiers in Oncology. 2022; 11: 789330.

[7] Alenezi WM, Fierheller CT, Recio N, Tonin PN. Literature Review of *BARD1* as a Cancer Predisposing Gene with a Focus on Breast and Ovarian Cancers. Genes. 2020; 11: 856.

[8] Hawsawi YM, Shams A, Theyab A, Abdali WA, Hussien NA, Alatwi HE, *et al*. BARD1 mystery: tumor suppressors are cancer susceptibility genes. BMC Cancer. 2022; 22: 599.

[9] Hu Q, Botuyan MV, Zhao D, Cui G, Mer E, Mer G. Mechanisms of BRCA1-BARD1 nucleosome recognition and ubiquitylation. Nature. 2021; 596: 438–443.

[10] Witus SR, Zhao W, Brzovic PS, Klevit RE. BRCA1/BARD1 is a nucleosome reader and writer. Trends in Biochemical Sciences. 2022; 47: 582–595.

[11] Tarsounas M, Sung P. The antitumorigenic roles of BRCA1-BARD1 in DNA repair and replication. Nature Reviews. Molecular Cell Biology. 2020; 21: 284–299.

[12] Zhang YQ, Bianco A, Malkinson AM, Leoni VP, Frau G, De Rosa N, *et al*. BARD1: an independent predictor of survival in non-small cell lung cancer. International Journal of Cancer. 2012; 131: 83–94.

[13] Zhang YQ, Pilyugin M, Kuester D, Leoni VP, Li L, Casula G, *et al*. Expression of oncogenic BARD1 isoforms affects colon cancer progression and correlates with clinical outcome. British Journal of Cancer. 2012; 107: 675–683.

[14] Li Q, Kaur A, Okada K, McKenney RJ, Engebrecht J. Differential requirement for BRCA1-BARD1 E3 ubiquitin ligase activity in DNA damage repair and meiosis in the Caenorhabditis elegans germ line. PLoS Genetics. 2023; 19: e1010457.

[15] Yu H, Gao G, Jiang L, Guo L, Lin M, Jiao X, *et al*. Decreased expression of miR-218 is associated with poor prognosis in patients with colorectal cancer. International Journal of Clinical and Experimental Pathology. 2013; 6: 2904–2911.

[16] Jabbari K, Cheng Q, Winkelmaier G, Furuta S, Parvin B. CD36^{+} Fibroblasts Secrete Protein Ligands That Growth-Suppress Triple-Negative Breast Cancer Cells While Elevating Adipogenic Markers for a Model of Cancer-Associated Fibroblast. International Journal of Molecular Sciences. 2022; 23: 12744.

[17] Ng L, Chow AKM, Man JHW, Yau TCC, Wan TMH, Iyer DN, *et al*. Suppression of Slit3 induces tumor proliferation and chemoresistance in hepatocellular carcinoma through activation of GSK3β/β-catenin pathway. BMC Cancer. 2018; 18: 621.

[18] Lee HS, Tamia G, Song HJ, Amarakoon D, Wei CI, Lee SH. Cannabidiol exerts anti-proliferative activity via a cannabinoid receptor 2-dependent mechanism in human colorectal cancer cells. International Immunopharmacology. 2022; 108: 108865.

[19] Livak KJ, Schmittgen TD. Analysis of relative gene expression data using real-time quantitative PCR and the 2(-Delta Delta C(T)) Method. Methods (San Diego, Calif.). 2001; 25: 402–408.

[20] Li W, Gu X, Liu C, Shi Y, Wang P, Zhang N, *et al*. A synergetic effect of BARD1 mutations on tumorigenesis. Nature Communications. 2021; 12: 1243.

[21] Terradas M, Capellá G, Valle L. Dominantly Inherited Hereditary Nonpolyposis Colorectal Cancer Not Caused by MMR Genes. Journal of Clinical Medicine. 2020; 9: 1954.

[22] Ozden O, Bishehsari F, Bauer J, Park SH, Jana A, Baik SH, *et al*. Expression of an Oncogenic BARD1 Splice Variant Impairs Homologous Recombination and Predicts Response to PARP-1 Inhibitor Therapy in Colon Cancer. Scientific Reports. 2016; 6: 26273.

[23] Zhang Y, Weinberg RA. Epithelial-to-mesenchymal transition in cancer: complexity and opportunities. Frontiers of Medicine. 2018; 12: 361–373.

[24] Lu W, Kang Y. Epithelial-Mesenchymal Plasticity in Cancer Progression and Metastasis. Developmental Cell. 2019; 49: 361–374.

[25] Saxena S, Purohit A, Varney ML, Hayashi Y, Singh RK. Semaphorin-5A maintains epithelial phenotype of malignant pancreatic cancer cells. BMC Cancer. 2018; 18: 1283.

[26] Jiang L, He C, Zhang X, Chen Y, Li G. MiR-193b-5p inhibits proliferation and enhances radio-sensitivity by downregulating the AKT/mTOR signaling pathway in tongue cancer. Translational Cancer Research. 2020; 9: 1851–1860.

[27] Peñalosa-Ruiz G, Bousgouni V, Gerlach JP, Waarlo S, van de Ven JV, Veenstra TE, *et al*. WDR5, BRCA1, and BARD1 Co-regulate the DNA Damage Response and Modulate the Mesenchymal-to-Epithelial Transition during Early Reprogramming. Stem Cell Reports. 2019; 12: 743–756.

[28] Duan X, Wang L, Wang Z, Wei W, Wang M, Ding D. LncRNA PGM5-AS1 Inhibits the Progression of Bladder Cancer by Regulating miR-587/SLIT3 Axis. Critical Reviews in Eukaryotic Gene Expression. 2022; 32: 9–22.

[29] Yang C, Gong J, Xu W, Liu Z, Cui D. Next-generation sequencing identified somatic alterations that may underlie the etiology of Chinese papillary thyroid carcinoma. European Journal of Cancer Prevention: the Official Journal of the European Cancer Prevention Organisation (ECP). 2023; 32: 264–274.

[30] Kim M, Kim JH, Baek SJ, Kim SY, Kim YS. Specific expression and methylation of SLIT1, SLIT2, SLIT3, and miR-218 in gastric cancer subtypes. International Journal of Oncology. 2016; 48: 2497–2507.